Available online at www.sciencedirect.com
SCIENCE DIRECT®
Proceedings of the Combustion Institute 30 (2005) 511–518
Proceedings of the Combustion Institute
www.elsevier.com/locate/proci

Gravity effects on partially premixed flames: an experimental-numerical investigation

Andrew J. Lock[a], Ranjan Ganguly[a], Ishwar K. Puri[b,*], Suresh K. Aggarwal[a], Uday Hegde[c]

[a] Department of Mechanical and Industrial Engineering (M/C 251), University of Illinois at Chicago, 842 W. Taylor St., Chicago, IL 60607-7022, USA
[b] Department of Engineering Science and Mechanics (MC 0219), Virginia Polytechnic Institute and State University, Blacksburg, VA 24061, USA
[c] National Center for Microgravity Research, Cleveland, OH, USA

Abstract

While premixed and nonpremixed microgravity flames have been extensively investigated, the corresponding literature regarding partially premixed flames (PPFs) is sparse. We report the first experimental investigation of burner-stabilized microgravity PPFs. Partially premixed flames with multiple reaction zones are established in microgravity on a Wolfhard–Parker slot burner in the 2.2 s drop tower at the NASA Glenn Research Center. Microgravity measurements include flame imaging, and thermocouple and radiometer data. Detailed simulations are also used to provide further insight into the steady and transient response of these flames to variations in g. The flame topology and interactions between the various reaction zones are strongly influenced by gravity. The flames widen substantially in microgravity. During the transition from normal to microgravity, the flame structure experiences a fast change and another relatively slower transient change. The fast response is due to the altered advection as the value of g is reduced, while the slow response is due to the changes in the diffusive fluxes. The radiative heat loss from the flames increases in microgravity. A scaling analysis based on a radiation Damköhler number is able to characterize the radiation heat loss.

1. Introduction

This is the first experimental investigation of burner stabilized partially premixed flames (PPFs) in microgravity (μg). PPFs are characterized by two or more reaction zones, of which at least one is chemically controlled and another transport-limited [1–4]. They are established when a rich fuel–air mixture at an equivalence ratio $\phi > 1$ burns in the presence of air or a lean fuel–air mixture ($\phi < 1$). Partial premixing occurs in numerous situations. For instance, lifted nonpremixed flames contain partially premixed regions [4,5], the reignition of locally extinguished regions during turbulent combustion often occurs under partially premixed conditions [6], and nonuniform evaporation in spray combustors, such as diesel engines, leads to partially premixed combustion [7]. This form of combustion may also be encountered in unwanted fires in space [8].

The various reaction zones of a PPF are synergistically coupled through the thermochemical

* Corresponding author. Fax: +1 504 231 4574.
E-mail address: ikpuri@vt.edu (I.K. Puri).

1540-7489/$ - see front matter © 2004 The Combustion Institute. Published by Elsevier Inc. All rights reserved.
doi:10.1016/j.proci.2004.08.144

and fluid mechanical interactions between them [9]. The rich ($\phi > 1$) zone is deficient in oxidizer, and thus dependent upon the lean ($\phi < 1$) region for supplemental oxygen. The lean premixed zone is aided by the supply of heat and radicals that sustain it even if the premixing level is below the lean flammability limit. The presence of the nonpremixed zone alters further the thermal and mass transport [10]. The complex velocity field produced by flow dilation and buoyant acceleration strongly influences these interactions between the reaction zones and thereby the flame topology.

Buoyancy enhances mixing between the rich and lean fuel/air streams. Its effect relative to the fluid inertia is characterized through the Froude number $Fr = v/(lg)^{1/2}$ (where v denotes velocity, l a characteristic length, and g is the gravitational acceleration). Thermal radiation from these flames is strongly coupled with the buoyancy and can be of considerable significance. Microgravity flames exhibit a greater lateral spread when buoyant acceleration decreases, thus increasing the flame volume [11], and the residence time of hot gases in the high temperature regions increases. Both of these factors lead to enhanced thermal radiation from μg flames.

2. Motivation and objectives

Law and Faeth [12], Kono et al. [13], and Ronney [14] have provided detailed reviews of experimental and computational studies dealing with premixed and nonpremixed 1 g and μg flames in different configurations. However, the corresponding literature regarding PPFs in μg conditions is sparse. Shu et al. [11] simulated the influence of buoyancy on double flames (PPFs containing two reaction zones). Azzoni et al. [9] conducted a similar investigation for triple flames. They observed that the enhanced oxidizer entrainment caused by buoyancy increased advective mixing and produced a more compact flame. These numerical results have not yet been validated. Motivated by this consideration, we present experimental results pertaining to burner stabilized double and triple PPFs. Numerical simulations were performed to provide further insight.

3. Experimental method

The μg experiments were conducted in the 2.2-s drop tower at the NASA Glenn Research Center in a self-contained drop rig. The rig is equipped with a Wolfhard–Parker slot burner. A schematic diagram of the burner [15] and a photograph of the drop rig are provided in Fig. 1. A rich methane–air mixture was introduced through the inner slot and a lean mixture or air through the outer

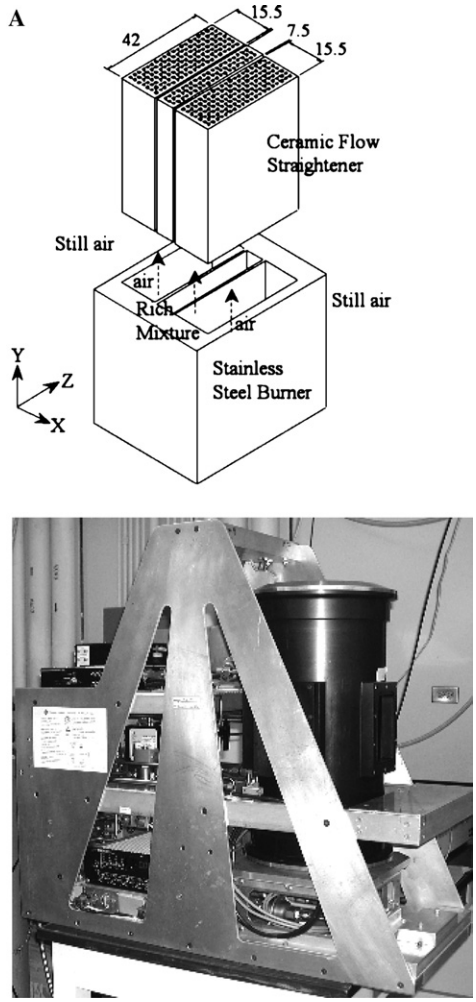

Fig. 1. (A) Wolfhard–Parker slot burner; and (B) the μg drop rig.

slots. A "drop" involved the process of preparing the rig, filling and mixing gases in onboard cylinders, loading and raising the rig to the top of the tower, initiating recording devices and computer controls, stabilizing the flame in 1 g for a few seconds, dropping the rig to achieve μg, and thereafter retrieving it. Gas flow and ignition were remotely initiated through timed computer controls, and the flame was observed through a video feed.

The flame images were recorded by at 30 frames/s an onboard CCD camera and an SVHS recorder. Temperature measurements were made using an array of eight 125-μm R-type thermocouples that were suspended at 5 mm axial increments and sampled at 50 Hz. Temperature measurements were made along the centerline, and at transverse displacements of 3, 5, 7, and 10 mm from it. A minimum of five drops was required to measure the

temperature field at a total of forty locations to characterize a single flame. The continual heating and cooling of the platinum wire caused the position of the suspended thermocouple bead to move by ±0.5 mm. The thermocouple measurements were corrected for radiation losses [16], and the uncertainties associated with the data are within ±10%. Radiation measurements were made using a small Schmidt–Boelter thermopile detector that had a Zinc Selenide window and a 150° view angle. The entire flame was included in the radiometer field of view.

4. Numerical method

The computational model is based on the algorithm developed by Katta et al. [17], and the simulation method is described in detail elsewhere [4,9–11,15,18]. The numerical model solves the time–dependent governing equations for unsteady reacting flows in a two-dimensional planar or axisymmetric configuration. in rectangular coordinates, these equations are

$$\frac{\partial(\rho\Phi)}{\partial t}+\frac{\partial(\rho u\Phi)}{\partial x}+\frac{\partial(\rho v\Phi)}{\partial y}=\frac{\partial}{\partial x}\left(\Gamma^{\Phi}\frac{\partial\Phi}{\partial y}\right)+\frac{\partial}{\partial y}\left(\Gamma^{\Phi}\frac{\partial\Phi}{\partial y}\right)+S^{\Phi}.$$

Here, t is the time, u and v represent the x and y velocity components, respectively. The general form of the equation represents conservation of mass, momentum, species, or energy conservation equation, depending on the variable used for Φ. The diffusive transport coefficient Γ^{Φ} and source terms S^{Φ} appearing in the above equation are provided in Table 1 of [4]. Introducing the overall species conservation equation and the state equation completes the set of equations. In addition, a sink term based on an optically thin gas assumption is included in the energy equation to account for thermal radiation in the flame [19]. According to the optically thin approximation, the sink term due to the radiation heat loss q_{rad} is $q_{\text{rad}}=-4\sigma K_p(T_4-T_0^4)$ [20]. where T denotes the local flame temperature. The term K_p accounts for the absorption and emission from the participating gaseous species (CO_2, H_2O, CO, and CH_4) and is expressed as $K_p=P\sum_k X_k K_{p,k}$, where $K_{p,k}$ denotes the mean absorption coefficient of the kth species. Its value is obtained by using a polynomial approximation to the experimental data provided in [21]. The methane–air chemistry is modeled using a detailed mechanism that considers 24 species and 81 elementary reactions [22]. The mechanism has been validated for the computation of premixed flame speeds and the structure of nonpremixed and PPFs [4,9–11,15,18,23–25].

Computations are performed in a Cartesian domain with planar symmetry. The origin is defined 2 mm below the burner lip at the burner centerline. The domain extends 0.1 m laterally and 0.15 m axially. Compared to a typical flame height and maximum width of 0.03 and 0.02 m, respectively, this domain is of reasonable size. A 100×200 grid with clustering near the centerline and the inlet plane (where the gradient in the field variables is large) was observed to produce grid independence.

5. Results and discussion

5.1. Global flame structure

The flame conditions were selected such that buoyancy and momentum effects were comparable at 1 g so that the Froude number (Fr) was ~1. For a typical 1 g flame, $v=30$ cm/s and $l=0.4$ cm (the characteristic lateral reaction zone dimension) for which $Fr=1.51$. Figure 2 presents images of double and triple PPFs obtained in (1) 1 g and (2) μg near the end of the drop. Visually, the μg flames appear to assume a quasi-steady shape within ~200 ms after releasing the rig; however, as noted later, their temperature and radiation fields keep evolving until the end of the drop.

For the double flames depicted in Figs. 2A and B, the momentum ratios of the inner to the outer flows are nearly identical. For both the cases, the flame contains two reaction zones—an inner rich premixed zone and an outer nonpremixed zone.

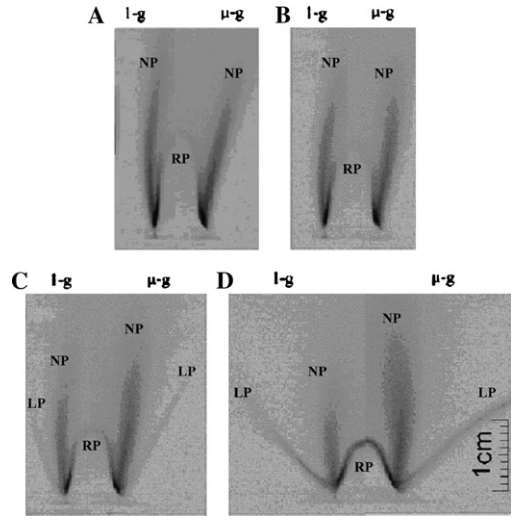

Fig. 2. Direct images of the double (A and B) and triple (C and D) flames at 1 g and μg (A) $\phi_{\text{in}}=2.38$, $\phi_{\text{out}}=0$, $V_{\text{in}}=21.2$ cm/s, $V_{\text{out}}=32.3$, (B) $\phi_{\text{in}}=1.68$, $\phi_{\text{out}}=0$, (C) $\phi_{\text{in}}=1.68$, $\phi_{\text{out}}=0.36$; and (D) $\phi_{\text{in}}=1.68$, $\phi_{\text{out}}=0.5$; for (B–D): $V_{\text{in}}=15.9$ cm/s, $V_{\text{out}}=25.8$ cm/s. (RP, rich premixed; NP, nonpremixed; and LP, lean premixed).

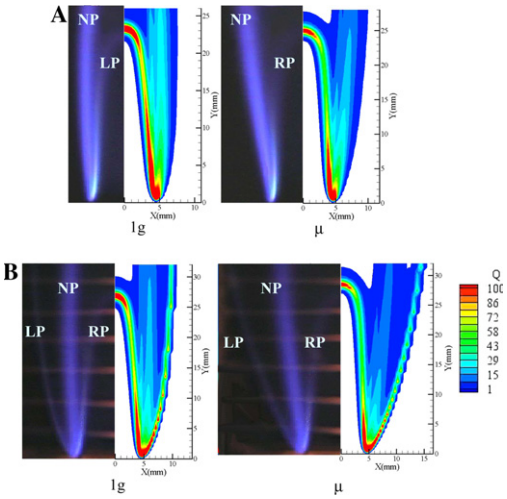

Fig. 3. Experimental (direct image) and numerically simulated heat release topologies (kJ/kg s: all rates above 100 kJ/kg s were clipped) of double and triple flames in 1 g and μg; (A) double flame ($\phi_{in} = 2.0$) and (B) triple flame ($\phi_{in} = 2.0$, $\phi_{out} = 0.35$). For both cases, $V_{in} = V_{out} = 30$ cm/s.

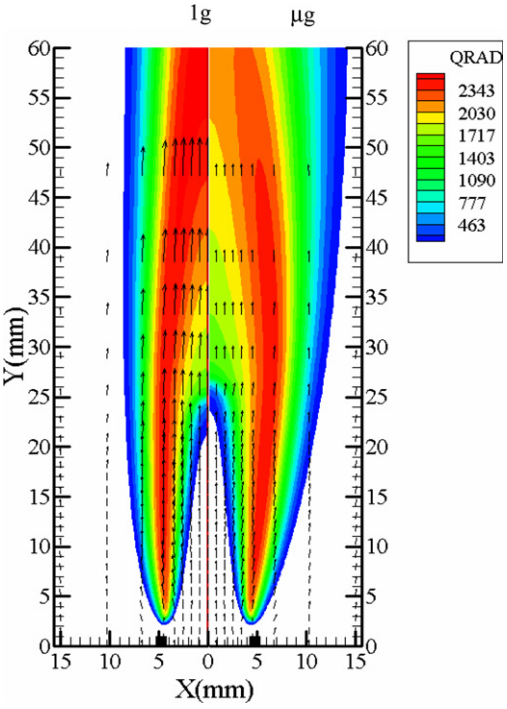

Fig. 7. Numerically predicted radiation contours (W/mm^2) and velocity vectors for a double flame at 1 g (left) and μg (right) ($\phi_{in} = 2.0$, $\varphi_{out} = 0$, $V_{in} = V_{out} = 30$ cm/s).

The outer nonpremixed reaction zone moves farther outward in μg for both conditions and, visually, the intensity at its tip weakens. In addition,

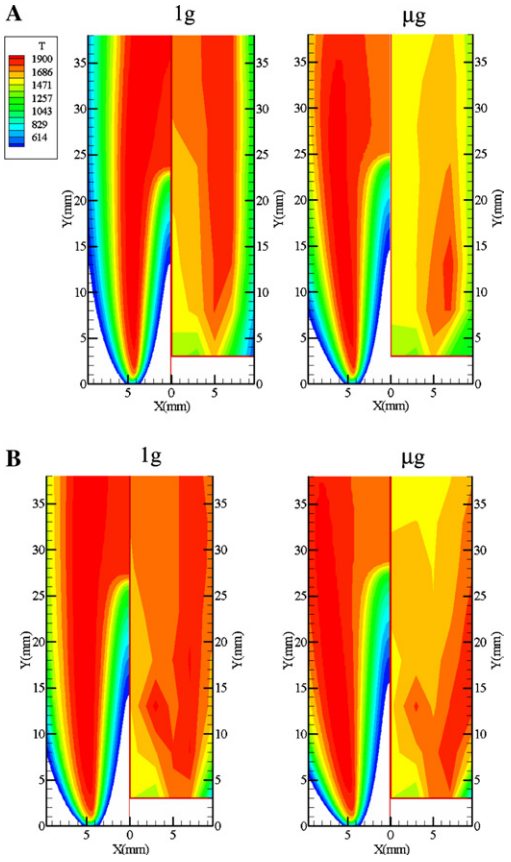

Fig. 4. Measured and predicted temperature (K) contours in 1 g and μg for the (A) double flame, $\phi_{in} = 2.0$, and (B) triple flame $\phi_{in} = 2.0$, $\phi_{out} = 0.36$. For both cases, $V_{in} = V_{out} = 0.3$ m/s.

there is a small increase in the height of the inner rich premixed zone and a slight weakening of its tip intensity in μg. The absence of buoyancy diminishes the oxidizer flux into the inner reaction zone. Consequently, the outer nonpremixed reaction zone moves laterally outward to meet its oxidizer demand. The spatial separation between the inner and outer reaction zones increases in μg, a result that is in accord with previous simulations [11].

The heights of the normal- and micro-gravity double flames presented in Fig. 2A are higher than those of the corresponding flames in Fig. 2B. This is due to the larger fuel flow rate in the former case. A closer observation of Figs. 2A and B reveals that the flame with a larger inner equivalence ratio ϕ_{in} exhibits a more pronounced lateral spread. Bennett et al. [26] have shown that a larger value of ϕ_{in} for a 1 g flame produces a greater oxidizer entrainment, most of which is buoyancy driven. Therefore, as a 1 g flame transits to μg, the loss of the buoyancy-induced flux has greater consequences for flames with greater ϕ_{in}.

Figure 2C presents images of a PPF with a triple flame structure in 1g and μg. A third reaction zone appears outside of the nonpremixed flame region as a result of lean premixing of the outer stream. This lean premixed zone spreads further outward in μg and reduces the influence of gravity on the inner reaction zones by producing a fluid dynamic shielding effect. Reducing the buoyancy leads to an increased separation between the three reaction zones [9]. For all the flames considered, increased gravitational acceleration makes the nonpremixed reaction zone more compact and spatially closer to the inner rich premixed zone. For instance, in Fig. 2D, the μg nonpremixed zone is approximately 20% longer and about 30% larger (at the point of greatest width) than in 1 g.

Figures 3A and B present a comparison of the predicted heat release rates with the experimentally obtained images for two representative PPFs in 1 g and μg, one with a double flame structure and the other a triple flame. The intrusive thermocouple array is visible in the triple flame image (Fig. 3B). However, the qualitative similarity observed between images of Figs. 2 and 3 indicates that the presence of the thermocouples has a negligible impact on the flame structure. The topologies of the reaction regions obtained from the experiments and simulations are in good agreement in both 1 g and μg. The heights of the inner reaction zones are well predicted. Both the simulated heat release rates and the chemiluminescence in the direct images along the sides of the inner (premixed) flame decrease due to stretch effects. The heat release rate progressively decreases along the outer (nonpremixed) flame at downstream locations. The nonpremixed reaction zone has a weak tip, and its reaction rates are larger in upstream regions. In addition, the measured and predicted shapes and widths of the two outer (nonpremixed and lean premixed) reaction zones are in good agreement for the triple flame.

5.2. Temperature and radiation measurements

The measured and simulated temperatures for the flames depicted in Figs. 3A and B are presented in Figs. 4A and B. The simulated and measured temperature profiles are expected to differ due to the intrusive nature of the thermocouples and uncertainties associated with the radiation corrections. (However, the implementation of nonintrusive diagnostics in μg facilities is not straightforward). Since the reaction zone topologies are in good agreement in Fig. 3, we have confidence in the simulated temperature data. Both sets of data, measured and simulated, exhibit a similar qualitative behavior in 1 g and μg. As g decreases, the high temperature regions, particularly the nonpremixed reaction zones, are cooled due to enhanced radiation. The spatial distribution of the high temperature zone changes in μg, which is consistent with the flame topography change. In both the flames the high temperature regions lie along the nonpremixed reaction zone, which is in accord with previous investigations [9,11]. The spatial distribution of the high temperature zone changes in μg, which is consistent with the flame topography change.

To examine the transition of partially premixed flames from 1g to μg, the transient temperature data recorded during the drop are presented in Fig. 5 at a transverse location $x = 5$ mm for the double flame of Fig. 3A. This location intersects the outer nonpremixed reaction zone in 1 g (which widens in μg). The data were smoothened by a 10-point moving average. The local temperatures experience an initial transient between 1.5 s (when the rig is released from 1 g) and 2 s in accord with the rapid initial changes in the flame topology after the rig is released. However, there is a second more gradual temperature change in μg that does not reach a steady state during the drop. The flame topologies in 1 g, during the 1 g to μg transition, and under quasi-steady μg conditions are also shown in the figure.

The temperature near the flame base at ($y = 3$ mm) is unchanged during the drop, since the diminishing buoyancy least influences this location. However, higher axial positions exhibit a progressively larger temperature decline during the drop (from $t = 1.5$ to 3.5 s) due to the outward spreading of the nonpremixed reaction zone and the increased significance of thermal radiation. The thermocouple time constant (~0.1 s) is of the same order as the duration of flame spreading (~0.2 s). The temperature decline during the initial transient period occurs during 0.5 s, but a gradual temperature decrease continues thereafter until the end of the drop.

Further insight can be provided by using a phenomenological or scale analysis that compares the advection time τ_c and the diffusion time τ_d for a representative flame (schematically described in the inset in Fig. 5). The characteristic fuel and

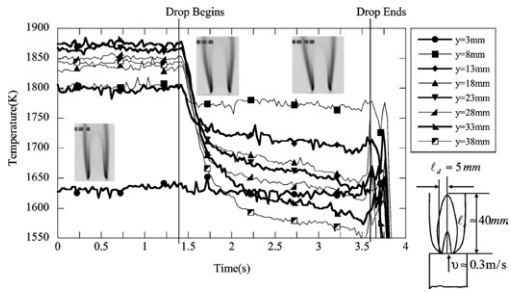

Fig. 5. Transient temperature data for a double flame at eight vertical (y) locations at 5 mm away from the plane of symmetry (i.e., $x = 5$ mm). $\phi_{in} = 2.0$, $\phi_{out} = 0$, $V_{in} = V_{out} = 30$ cm/s (inset: schematic of characteristic flame scales).

air velocities v are assumed to be equal. The transit or convective time is $\tau_c = l_c/v$, and the diffusion time required for the reactants to be transported laterally through the flame is $\tau_d = l_d^2/D$. For the flames considered, the characteristic length scales are $l_c \sim 40$ mm and $l_d \sim 5$ mm, $v \sim 0.3$ m/s, and the diffusivity $D \sim 1.3 \times 10^{-5}$ m^2/s so that $\tau_c \sim 0.1$ s and $\tau_d \sim 1$ s. This implies that the rapid temperature decline during the first 0.5 s occurs due to changes in the advection as the flame transitions from 1 g to μg. The diffusive flux adjusts to the corresponding changes in the flame structure and produces the second more gradual transient. The value of τ_d is of the order of the duration of the experiment. (The μg data in Fig. 4 represent a condition near the end of the drop at which that the temperature field closely resembles that for a steady state μg flame.)

Figure 6 presents radiometer measurements for a characteristic triple flame during the drop. The plot is normalized with respect to the measurement made just following ignition at $t = 0$. The flame is in a steady state before the rig is dropped. Because of the integrated nature of the radiation measurement, only the slower diffusive transient discussed above is readily discernable from the data. As the gravitational acceleration decreases during the drop, the radiation heat transfer from the flame increases significantly. Similar effects of gravity on radiation have been observed for nonpremixed flames [27]. The measurement at the end of the drop is approximately 35% larger than when it commences.

The measured peak flame temperature for the double flame decreases by ~0.7% and for the triple flame by ~2.1% in μg. We can also define a mean temperature as the averaged value of all thermocouple measurements. Unlike the peak flame temperature, this mean temperature increases by ~0.6% for the double flame and ~3.8% for the triple flame. Although the peak flame temperature in a μg flame is lower, the radiative heat transfer originates from a larger overall flame volume with a somewhat higher average

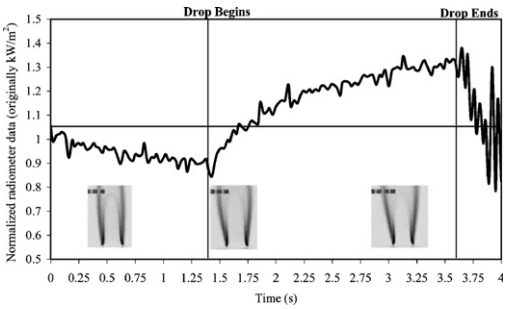

Fig. 6. Measured radiometer data during the drop for the flame showing the transient response of flame radiation. Flame conditions correspond to that of Fig. 3A.

temperature. We attribute this to the smoothening of temperature gradients in μg due to a widening of the flame volume and an increase in the relative importance of diffusion [9,11].

Qin et al. [19] employed an optically thin radiation model in their detailed simulations and predicted a similar temperature decrease for double flames. Figure 7 presents a comparison of the local volumetric radiation loss q_R''' for the 1 g and μg double flames shown in Fig. 3. Since the radiation model accounts for the locally varying gas emissivities, the radiation field differs from the temperature distribution, i.e., there is an absence of strict one-to-one correspondence between locations of high temperature and large radiation. The peak value of q_R''' decreases as the flame transits from 1 g to μg. However, except for a few large values of q_R''', the iso-q_R''' lines occupy a larger area in the μg flame. Therefore, integrating q_R''' over the entire domain yields a larger total value of the radiation heat flux for the μg flame. The global radiative heat fraction χ_R (which is the ratio of the total radiative heat transfer from the flame to the total heat liberated due to combustion) increases from 21.7% at 1 g to 47.3% at μg for the flames discussed in Fig. 7. They both burn the same amount of fuel and generate an identical amount of heat.

The μg flame has a lower peak temperature but a larger width. Therefore, it experiences a smaller transverse temperature gradient, which leads to lower conduction heat transfer from it than for the corresponding 1 g flame. Thus, the 117% increase in radiation heat transfer and decrease in conduction in μg is accompanied by a commensurate reduction in the convective heat loss from the flame. In addition, in the absence of buoyancy, the gas velocity in the post-flame region is much smaller (as shown by the velocity vectors in Fig. 7) than in a buoyant flame.

The effect of microgravity on the flame radiation can be analyzed by defining a radiation cooling time τ_R. It is defined as the time required for a gas volume temperature to decrease from an initial value T_f, by an amount, dT, where $\tau_R = T_f/(dT/dt) \approx T_f/(Q_R/(\rho c_p))$. Here, $Q_R = (Q_{gen} - Q_c)$ denotes the radiation heat transfer, ρ density, and c_p the heat capacity. The radiation (fourth) Damköhler number compares the heat generated to the heat lost through radiation, i.e., $Da_R = Q_{gen}/Q_{loss} \sim \tau_R/\tau_c$. As $Da_R \to 1$, the radiation heat loss becomes more significant. The value of τ_c is related to the time taken by the gas to flow through the radiating volume. If the characteristic velocity is to account for the contribution of buoyant acceleration, then $v = v_{in} + v_b = v(g)$, where v_{in} and v_b represent the velocities at the burner exit and the corresponding buoyancy-induced component, respectively.

It is possible to show that $\tau_R \sim l(X_f Q_{HV}/c_p T - 1)^{-1} = f(X_f, T^{-1})$, where Q_{HV} denotes the

heat of reaction of the fuel and X_f the fuel mole fraction. Therefore, $Da_R \sim \tau_R/\tau_c \sim v(g)\ f(X_f, T^{-1})$, where T is a function of X_f. The relative radiative loss increases with a decrease in the value of $v(g)$ or at larger values of T, as expected. An alternate expression for $Da_R \sim (v_{in}/v_{in} + v_{in}/v_b)\ f(X_f, T) \sim (1 + Fr^{-1})\ f(X_f, T^{-1})$ illustrates its variation with the Froude number. As Fr increases (during the transition from 1 g to μg), the value of Da_R decreases, i.e., the relative significance of radiation increases. For a constant inlet stream velocity, this formulation represents the fractional radiative loss as a function of g.

The variation of χ_R (or $\sim 1/Da_R$) obtained from the scaling analysis with respect to g is plotted in Fig. 8. The analysis shows that the radiative loss fraction significantly increases with decreasing values of g. The relative increase in the radiation loss is most prominent in the range 0–1 g (which corresponds to the radiometer data presented in Fig. 6). The scaling analysis assumes a constant effective temperature that is representative for the entire domain, and which is expected to change with varying gravitational acceleration. Nonetheless, the analysis provides insight into the influence of buoyancy on the radiation heat loss from the flame. As shown above, that temperature variation is small and of the order of 1% for the flames examined herein.

The figure also presents the variation of χ_R obtained from the simulations that were performed for twenty values of g (in the range 1–100 g), keeping all other conditions identical to those for the flames in Fig. 3A. The simulated values of χ_R with respect to g follow a trend that is similar to that obtained from the scaling analysis. While the simulated values are based on an exact determination of χ_R, the calculated values from the scaling analysis assume a constant effective mean flame temperature whose value depends on the chosen length scale (i.e., the dimensions over which the temperatures are averaged). For a given stoichiometry and flowrates, the curves in Fig. 8 emphasize the relative importance of radiation for different levels of gravitational acceleration and mean domain temperature (which can be a function of air/fuel preheating, oxygen enrichment, etc.). Such a relationship is, therefore, useful to predict the flame behavior for fundamental phenomena (e.g., to predict radiation quenching) or for thermal design (e.g., to determine the radiant surface areas for utility furnaces) for various values of g. The simulations show that $\chi_R \sim 47\%$ at 0 g, 27% at 0.5 g, 22% at 1 g, 17% at 2 g, and 12% at 5 g. The effective temperatures that reproduce these results in the scaling analysis lie in the relatively narrow range from 900 to 1080 K.

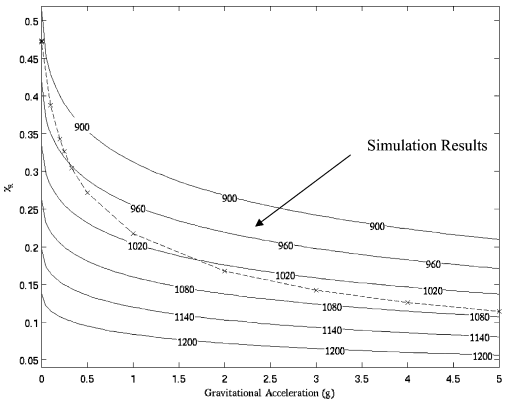

Fig. 8. Variation of the global radiative heat fraction (χ_R) from a double flame with gravitational acceleration (g) for different temperatures. Results from the scaling analysis for a representative temperature range of 900–1080 K show close agreement with the numerical predictions.

6. Conclusions

In this paper, we report an experimental–numerical investigation of burner-stabilized μg partially premixed flames. Both the steady and transient characteristics of these flames are examined under 1 g and μg conditions.

The flame structure is strongly influenced by buoyancy, which reduces the spatial separation between the reaction zones, and, thus, increases interactions between them. While the structure and location of the inner rich premixed zone is relatively insensitive to the variation in g, the non-premixed zone and the outer lean premixed zone (in the case of triple flame) are strongly influenced by g.

Measurements and simulations show good agreement with respect to flame topology and locations of the various reaction zones. The computed and measured temperature profiles are qualitatively consistent although they exhibit some quantitative differences due to the intrusive nature of the thermocouples and uncertainties associated with the radiation corrections.

During the transition from 1 g to μg, the flame structure experiences a rapid change and another a relatively slower transient change. The faster transient stabilizes within 200 ms and is due to changes in advection caused by reduced gravity. The slower transient does not fully stabilize in the available μg time. It is attributed to changes in the diffusive fluxes in response to the change in advection.

The effect of gravity on thermal radiation loss from PPFs has been characterized. The thermal radiation from these flame increases significantly in μg. This is due to the larger flame volume and the reduced advective heat flux in μg. A scaling analysis is presented that explains the results and

provides a useful estimate the flame radiation at various values of g.

Acknowledgments

This research was supported by the NASA Glenn's Microgravity Science Division (Dr. Kurt Sacksteder, Program Manager) through Cooperative Agreement No. NCC3-688. AL was supported by Fellowships through the NASA Graduate Student Research Program and the UIC Graduate College.

References

[1] I. Yamaoka, H. Tsuji, *Proc. Combust. Inst.* 15 (1974) 637–644.
[2] K. Seshadri, I. Puri, N. Peters, *Combust. Flame* 61 (1985) 237–249.
[3] C.K. Law, T.X. Li, S.H. Chung, J.S. Kim, D.L. Zhu, *Combust. Sci. Technol.* 64 (1989) 199–232.
[4] Z. Shu, S.K. Aggarwal, V.R. Katta, I.K. Puri, *Combust. Flame* 111 (1997) 276–295.
[5] M.D. Smooke, K. Seshadri, I.K. Puri, *Proc. Combust. Inst.* 22 (1988) 1555–1563.
[6] N. Peters, *Proc. Combust. Inst.* 20 (1984) 353–360.
[7] P.F. Flynn, R.P.Durrett, G.L. Hunter, A.O. Loye, O.C. Akinyemi, J.E. Dec, C.K. Westbrook, *SAE Paper* 1999-01-0509 (1999).
[8] C.K. Law, G.M. Faeth, *Prog. Energy Combust. Sci.* 20 (1994) 65–113.
[9] R. Azzoni, S. Ratti, I.K. Puri, S.K. Aggarwal, *Phys. Fluids* 11 (1999) 3449–4000.
[10] X. Qin, I.K. Puri, S.K. Aggarwal, *Phys. Fluids* 40 (2001) 731–740.
[11] Z. Shu, C.W. Choi, S.K. Aggarwal, V.R. Katta, I.K. Puri, *Combust. Flame* 118 (1999) 91–107.
[12] C.K. Law, G.M. Faeth, *Prog. Energy Combust. Sci.* 20 (1994) 5–113.
[13] M. Kono, K. Ito, T. Niioka, T. Kadota, J. Sato, *Proc. Combust. Inst.* 26 (1996) 1189–1199.
[14] P.D. Ronney, *Proc. Combust. Inst.* 27 (1998) 2485–2506.
[15] Z. Shu, B.J. Krass, C.W. Choi, S.K. Aggarwal, V.R. Katta, I.K. Puri, *Proc. Combust. Inst.* 27 (1998) 625–632.
[16] S. Ratti, *An Experimental Study on the Structure of Triple Flames Stabilized on a Slot Burner*, MS thesis, UIC, 1999.
[17] V.R. Katta, L.P. Goss, W.M. Roquemore, *Combust. Flame* 96 (1994) 60–74.
[18] Z. Shu, V.R. Katta, I.K. Puri, S.K. Aggarwal, *Combust. Sci. Technol.* 157 (2000) 185.
[19] X. Qin, S.K. Aggarwal, I.K. Puri, V.R. Katta, *AIAA 41st Aerospace Science Meeting and Exhibit, Jan 6-9, 2003, Reno, Nevada*, Paper No. AIAA-2003-1018.
[20] R. Siegel, J.R. Howell, *Thermal Radiation Heat Transfer*. Hemisphere Publishing New York, 1981.
[21] N. Smith, J. Gore, J. Kim, Q. Tang, *Radiation Models, International Workshop on Measurement and Computation of Turbulent Nonpremixed Flames*. Available from: <http://www.ca.sandia.gov/tdf/Workshop/Submodels.html> 2001.
[22] N. Peters, Reduced kinetic mechanisms for applications in combustion systems, in: N. Peters, B. Rogg (Eds.), Lecture Notes in Physics, vol. m15. Springer, Berlin, 1993, pp. 3–14.
[23] H. Xue, S.K. Aggarwal, *Effects of reaction mechanisms on structure and extinction of partially premixed flames*, *AIAA J.* 39 (2001) 637.
[24] X. Qin, I.K. Puri, S.K. Aggarwal, *Proc. Combust. Inst.* 29 (2002) 1565–1572.
[25] X. Qin, X. Xiao, I.K. Puri, S.K. Aggarwal, *Combust. Flame* 128 (2002) 121–132.
[26] B.A.V. Bennett, C.S. McEnally, L.D. Pfefferle, M.D. Smooke, *Combust. Flame* 123 (2000) 522–546.
[27] M.Y. Bahadori, D.P. Stocker, U. Hegde, *Combust. Sci. Technol.* 167 (2001) 169–186.

Comment

Chih-Jen Sung, Case Western Reserve University, USA. Experimentally, do the partially premixed flames reach steady state within 2.2–5 s when subjected to step change in gravity? If not, what is the typical relaxation time based on your computational results?

Reply. Our temperature measurements show that the flames in the 2.2 s drop tower experiments do not reach a steady state. Published simulations from our group also support the observation that the flames are near, but not at, steady state at the end of that duration [1].

Reference

[1] X. Qin, I.K. Puri, S.K. Aggarwal, V.R. Katta, *Phys. Fluids* 16 (2004) 2963–2974.